

- and/or collisional scattering in the compressed capsule core (Figs. 1 to 3).
23. R. D. Petraso *et al.*, *Phys. Rev. Lett.* **90**, 095002 (2003).
24. C. K. Li *et al.*, *Phys. Rev. E* **80**, 016407 (2009).
25. T. A. Lasinski *et al.*, *Rev. Mod. Phys.* **45**, S1 (1973).
26. J. J. MacFarlane, *J. Quant. Spectrosc. Radiat. Transf.* **81**, 287 (2003).

27. This work was supported in part by the U.S. Department of Energy and the Laboratory for Laser Energetics (LLE) National Laser User's Facility (DE-FG52-07NA28059 and DE-FG03-03SF22691), Lawrence Livermore National Laboratory (B543881 and LDRD-ER-898988), CEADIF (France, Cooperative agreement DE-FC52-08NA28302), LLE (414090-G), Fusion Science Center at University of

Rochester (412761-G), and General Atomics (DE-AC52-06NA27279).

9 December 2009; accepted 15 January 2010  
Published online 28 January 2010;  
10.1126/science.1185747  
Include this information when citing this paper.

# Deglacial Meltwater Pulse 1B and Younger Dryas Sea Levels Revisited with Boreholes at Tahiti

Edouard Bard,\* Bruno Hamelin, Doriane Delanghe-Sabatier

Reconstructing sea-level changes during the last deglaciation provides a way of understanding the ice dynamics that can perturb large continental ice sheets. The resolution of the few sea-level records covering the critical time interval between 14,000 and 9,000 calendar years before the present is still insufficient to draw conclusions about sea-level changes associated with the Younger Dryas cold event and the meltwater pulse 1B (MWP-1B). We used the uranium-thorium method to date shallow-living corals from three new cores drilled onshore in the Tahiti barrier reef. No significant discontinuity can be detected in the sea-level rise during the MWP-1B period. The new Tahiti sea-level record shows that the sea-level rise slowed down during the Younger Dryas before accelerating again during the Holocene.

Understanding the behavior and predicting the fate of large ice sheets can be done in parallel by studying recent and ongoing changes in the climate system (1, 2) and by studying the dramatic sea-level changes that occurred during the last deglaciation [21,000 to 5000 years before the present (yr B.P.)]. To date, the most complete record of deglacial sea level is based on reef cores drilled at Barbados, which have yielded ages from both  $^{14}\text{C}$  (3–5) and mass spectrometric U-Th methods (5–8). The Barbados record is characterized by two periods of sea-level acceleration [meltwater pulses (MWP) 1A and 1B] that occurred around 14,000 calendar yr B.P. (cal yr B.P.) and 11,300 cal yr B.P., respectively. During each MWP event, the sea level apparently rose by several meters per century, leading to a major hydrological perturbation that probably impacted the ocean circulation [e.g., (9, 10)]. Both the amplitude and the localization of injection into the ocean are crucial in understanding the climatic impact of a MWP event [e.g., (11)]. However, several first-order questions remain unresolved on the precise characterization of these events, despite the intensive research carried out over the last decade (see SOM text 1).

The precise timing and amplitude of MWP-1A and 1B are still open questions, because both of these events were originally detected as

hiatuses between individual drill cores collected at different depths off Barbados (see SOM text 2 and map in fig. S2). Several other records have been interpreted later as direct or indirect evidence of the occurrence of MWP-1A (12–16). One of the main goals of the recent Integrated Ocean Drilling Program (IODP) Leg 310 at Tahiti was specifically to collect an additional coral record over the MWP-1A time window. The new suite of coral samples collected during this IODP campaign successfully confirms the existence of MWP-1A and leads to a reassessment of its age and amplitude (17).

However, MWP-1B is even more controversial and still needs to be confirmed, both at Barbados and at other far-field sites. Indeed, subsequent coral studies at Huon Peninsula (18) and Tahiti (12) questioned the timing and amplitude of this freshwater pulse. Additional doubts were also raised about the existence of MWP-1B by a study of sea level in northwest Scotland based on the so-called “marginal basin isolation” technique (19). However, the interpretation of this Scottish record is complex due to its proximity to former ice sheets in a region where the postglacial rebound contribution is dominant, which explains why the local sea level continued to fall during most of the deglaciation. So far, the sample coverage and depth resolution of these different studies are still insufficient to reach a definitive conclusion about MWP-1B. Unfortunately, the new IODP sample collection from Tahiti is of little help in studying MWP-1B, because the depth range of the drill cores was targeted on MWP-1A and the earliest part of the deglaciation (i.e., 90 to 120 m). At these depths, only deep-living coral species

persisted in the reef at the levels corresponding to the age of MWP-1B.

To settle the issue, we dated by U-Th 47 pristine coral samples from three new reef cores (P8, P9, and P10) drilled onshore of the Papeete barrier reef in Tahiti, close to the location of our previous study (23 U-Th dated corals from P6 and P7 cores) (12). P8 is at about the same position as P7 (12) but was drilled at an angle of 33° toward the sea, whereas P9 and P10 were collected in the inner part of the barrier reef toward the Papeete Pass (fig. S1).

Figure 1B shows a comparison of the new U-Th data from P8, P9, and P10 cores with the previous Tahiti record (12). Unlike the Barbados cores, each of these Tahiti cores yields an uninterrupted record of the time window corresponding to MWP-1B. The new U-Th data (Fig. 1B and table S1) provide an unprecedented resolution and can be compared to the other sea-level records from Barbados (7, 8), Papua New Guinea (Huon Peninsula) (18, 20), and Vanuatu (Urelapa) (21) (Fig. 1, C and D). The North Greenland Ice Core Project (NorthGRIP) isotope record is also plotted in Fig. 1A using its most recent time scale (22). This is done to compare the sea-level records with climatic transitions such as the inception and the end of the Younger Dryas (YD), which marks the start of the Holocene period.

The large number of data points derived from the four cores provides a very accurate constraint on the sea-level rise during this period, defined by the coherent upper envelope of the paleo-depths of the samples. The small scatter of the data reflects the inherent uncertainty linked to the paleo-bathymetry of corals and associated shallow-living biological assemblages (23, 24). Part of this overall scatter is also related to the different positions of the drill cores on the barrier reef (SOM text 2 and fig. S1). P9 and P10 record the upper reef crest on the inner part of the barrier. By contrast, P8 was drilled on the outer part of the barrier reef, with a deviation of 33° toward the sea. Therefore, in the lower sections of P8 below 65 m, the corals (red points in Fig. 1B) plot slightly lower than those from P7, P9, and P10, a difference that remains small (<6 m) but fairly systematic.

The rate of sea-level rise at Tahiti can be calculated by means of linear fits over the three specific climatic intervals: before, during, and after the YD event (thick lines in Fig. 1B) (see SOM text 2 and table S2 for details). Taken together, the Tahiti data define a relatively smooth sea-level rise, with no significant acceleration during the time interval corresponding to

Centre Européen de Recherche et d'Enseignement des Géosciences de l'Environnement (CEREGE), UMR 6635 CNRS, University Aix-Marseille, Institut de Recherche pour le Développement, Collège de France, Europôle de l'Arbois, BP 80, F-13545 Aix-en-Provence Cedex 4, France.

\*To whom correspondence should be addressed. E-mail: bard@cerge.fr

MWP-1B at Barbados (11,400 to 11,100 cal yr B.P.; area shaded green in Fig. 1). This conclusion is based on *Acropora* and *Pocillopora* samples from the four cores P7, P8, P9, and P10 (table S1), which exhibit a rather small scatter (<6 m) (see Fig. 1B). In contrast to the Tahiti record, the MWP-1B event appears as a prominent step of ~15 m between two drill cores at Barbados, implying an apparent rise of

~40 mm/year (Fig. 1D). In the Huon record, the time interval of MWP-1B falls within a time gap of about a millennium (12,100 to 11,100 cal yr B.P.). The Vanuatu record has only two coral samples in this interval, but even considering the few samples below (older) and above (younger), it remains difficult to pick out a step or pause during the 13,000 to 10,000 yr B.P. interval. Therefore, both records from Pacific

far-field sites agree with the higher resolution record from Tahiti: None of these reconstructions shows an abrupt 15-m step around 11,300 cal yr B.P., in contrast to the Barbados record.

The new Tahiti record includes many samples covering the YD cold period, in particular from cores drilled in the inner part of the outer reef (P9 and P10). An important observation based on this data set is that the deglacial sea-level rise slowed down during the YD event and reaccelerated during the early Holocene ( $7.5 \pm 1.1$  mm/year during the YD, compared with  $11.7 \pm 0.4$  mm/year after and  $12.1 \pm 0.6$  mm/year before). Similar conclusions can be derived (see details in SOM text 2 and table S2) by considering the data obtained on the shallow-living corals (*Acropora* and *Pocillopora*, dots in Fig. 1B) or by looking at the entire data set, including those measured on more ubiquitous corals (*Porites* and *Favidea*, triangles in Fig. 1B). The Barbados record also suggests that the rate of sea-level rise was reduced to  $5.6 \pm 0.4$  mm/year (Fig. 1D and table S2), in agreement with the slowing down observed for Tahiti. The case for a slower sea-level rise during the YD event than during the period immediately before ( $9.3 \pm 0.4$  mm/year) is particularly strong because all *A. palmata* samples come from the very same Barbados drill core #12 (in contrast to MWP-1B, which occurs between Barbados cores #12 and #7). The existence of a transient pause in the deglacial sea-level rise was also suggested by considering samples older and younger than the 12,100 to 11,100 cal yr B.P. data gap in the Huon record (18). Between 12,100 and 11,100 cal yr B.P., the sea-level rise clearly slowed down, although the data gap in the Huon record does not correspond exactly to the YD event and makes it difficult to compare with records from other sites.

In addition, the coral data plotted in Fig. 1 could suggest a small step (<6 m) in sea level near the onset of the YD event at around 13,000 yr B.P. (arrow in Fig. 1). This small step also corresponds to a rate change in both the Barbados and Tahiti records. At Huon, this period is covered by only a few corals that could possibly be fitted with a small step. However, the existence of such a structure is within the overall uncertainty of the approach (see details in SOM text 2) and thus remains speculative.

Relative sea level (RSL) differences between the records obtained for different sites should be interpreted with caution because isostatic effects are not the same everywhere on the planet. Therefore, a more complete comparison between these reconstructions of local sea-level records requires geophysical modeling. Milne and Mitrovia (25) drew up a comprehensive comparison by using a wide range of mantle viscosity and lithospheric models forced by different ice-sheet histories. These model simulations illustrate systematic differences in RSL between the different sites: In the time window of interest, the shallowest sea level should be

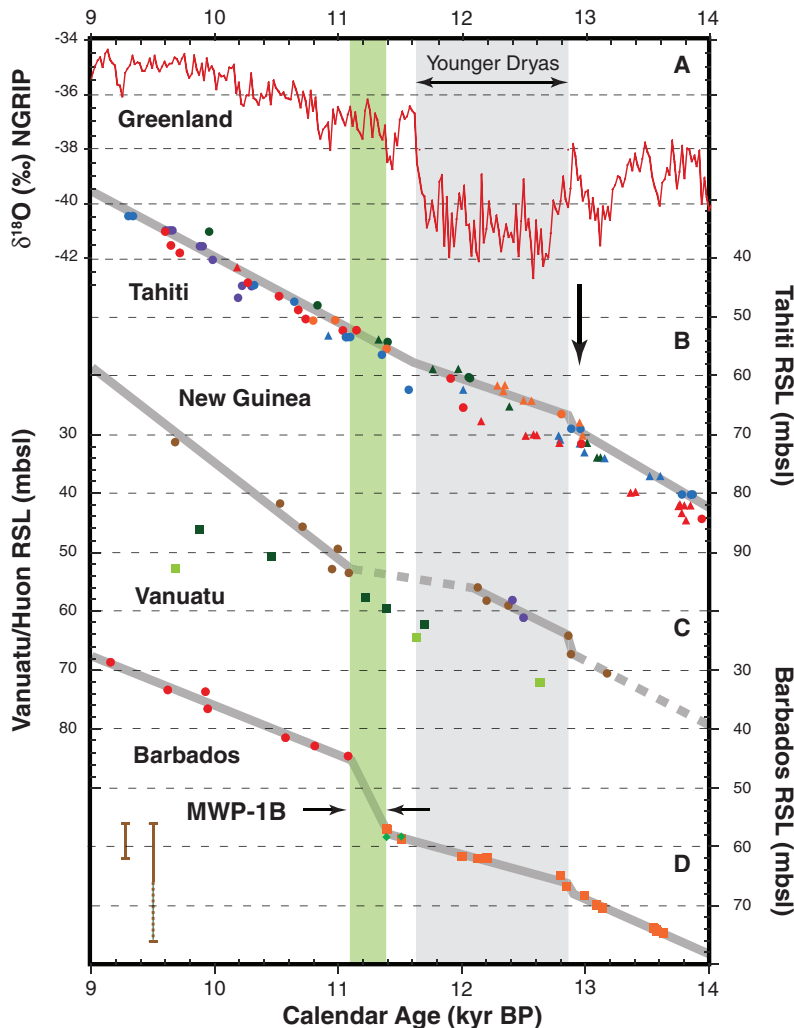


**Fig. 1.** Deglacial records over the 14,000 to 9000 yr B.P. time window. (A)  $\delta^{18}\text{O}$  record of the NorthGRIP Greenland core plotted on its most recent time scale (22). (B) Tahiti corals: depth in meters below present sea level versus U-Th ages in thousand years B.P. (core P6, dark blue; P7, light blue; P8, red; P9, orange; P10, green) (see table S1). (C) Pacific corals from Huon Peninsula, Papua New Guinea [brown dots (18), blue dots (20)] and from Urélapa, Vanuatu [light and dark green squares correspond to two different cores (21)]. (D) Barbados *A. palmata* corals [core #12, orange squares; core #7, red dots; core #16, green diamonds (8)]. All depths have been corrected for subsidence (Tahiti) and uplift (all other sites) as described in SOM text 2. Shaded time windows correspond to the YD [boundaries based on (A)] and to the MWP-1B event [boundaries based on (D)]. For Tahiti, the species and/or genus of the dated corals are provided in table S1. The bathymetric habitat of *Acropora* with *Pocillopora* [dots in (B)] is more restricted (about 6 m, a range shown by the short brown bar in the lower left corner) than those of *Porites* or *Favidea* corals [triangles in (B)], which can live in the top 10 to 20 m (a range shown by the longer brown bar in the lower left corner). Dark gray lines correspond to linear fits of sea-level data (SOM text 2 and listed in table S2). For Tahiti, the calculations exclude samples from the base of the P8 core deviated toward the shore (red dots below ~65 m) and samples made of *Porites* or *Favidea* corals. Using other assumptions would not change significantly the calculated rates of sea-level changes and would not change our conclusions (SOM text 2 and table S2). For New Guinea, dashed lines are used when data are scarce (gap starting in the middle of the YD and period before YD).

observed at Huon and the deepest at Barbados, whereas Tahiti RSL falls in between. This is in good agreement with the observations: At 12,000 cal yr B.P., the RSL is situated at 62, 59, and 55 m below modern sea level for Barbados, Tahiti, and Huon, respectively.

Geophysical processes, such as gravitational and rotational effects, can also affect the relative amplitude of abrupt sea-level changes expressed as steps in RSL records (26). Clark *et al.* (11) even proposed that comparing such steps at different sites could serve to identify the ice sheet(s) that released large amount of icebergs or meltwater. The apparent discrepancy between the Barbados and Tahiti records over the MWP-1B period around 11,300 cal yr B.P. may be reconciled by assuming that the ice was released exclusively from the Pacific sector of the Antarctic ice sheet (11, 26). However, in this scenario, the model predicts that a small residual step should be expected at Tahiti. Our data suggest that this step would be masked by the inherent uncertainty linked to the coral approach (less than 6 m). Further postglacial rebound modeling simulations such as (11, 26) should be performed to investigate whether such a scenario could generate steps larger than 10 m at Barbados and less than 6 m at Tahiti, a relative gradient even larger than the one caused by a release from the West Antarctica Ice Sheet (11, 26). This hypothetical scenario would also require that the Antarctic ice sheet was much larger than today during the glacial period. This issue has been controversial, but recent numerical modeling of the Antarctic ice sheet (27) is compatible with a total loss of ice of 17.5 m of equivalent sea level since 15,000 yr B.P. (including both contributions of MWP-1A and MWP-1B). However, specific attempts of geophysical modeling focused on the specific contribution to MWP-1B (28, 29) failed to reconcile the observed contrast in RSL with a reasonable contribution from the Antarctic ice sheet [see figure S3 in (29)]. Another puzzling aspect of MWP-1B is the lack of clear signals in marine sediments, from the Southern Ocean or the North Atlantic, for a large freshwater release to the Ocean that should have been similar to the Heinrich events.

Otherwise, we should consider the alternative possibility that MWP-1B might have been overestimated at Barbados. Mapping site locations on the Barbados south coast shows that cores defining MWP-1B are drilled in different environments: submerged fossil barrier reef for the deepest cores #12 and 16, and fringing reef for the shallow core #7 (map in fig. S2). A systematic bathymetric difference between both environments could be invoked, but this hypothesis would imply that, during the sea-level transition, the depth tolerance of *A. palmata* exceeded its 5-m limit, observed during the modern period characterized by sea-level stability. An additional cause of the bias might be the local tectonics of Barbados. Due to its location on the accretionary prism at the convergent

boundary between the Caribbean and South American plates, Barbados is characterized not only by a general uplift of varying amplitude around the island but also by several faults and tectonic flexures (30). It is thus probably an oversimplification to apply a constant uplift rate to all samples. Indeed, the position of cores #12 (#16) and #7 suggests that they may belong to different neotectonic segments (map in fig. S2) and thus were affected by different uplift rates. Nevertheless, it seems very unlikely that this tectonic factor could explain the full amplitude of the jump observed in the coral record, since even tripling the differential uplift correction between the cores would only contribute to half of the 15-m sea-level step observed at Barbados (see SOM text 2 for a full discussion of this issue). In principle, the different explanations invoked to explain the Barbados step (East Antarctic release and local biases at Barbados) are not mutually exclusive and could have been superimposed, but it seems rather unlikely that all these independent processes occurred within the same time window of a few centuries.

In addition to the absence of a detectable MWP-1B step at Tahiti, the other conclusion of our study, that the rate of sea-level rise was reduced during the YD period and reaccelerated during the early Holocene, has often been overlooked. This scenario would resolve the long-standing controversy between the observation of a slower rate of sea-level rise during the YD and the hypothesis that this millennium-long cold event was triggered by a meltwater pulse that slowed the Atlantic meridional overturning circulation. Our new record is compatible with previous modeling work (10) mentioning a reduced sea-level rise during the YD and briefly discussing the climatic implications with respect to freshwater forcing. The detection of a small sea-level change just before the start of YD at ~13,000 yr B.P. is tempting but remains difficult to prove. The reduced rate of sea-level rise observed during the following millennium (i.e., the YD event) would then correspond to a return of glacial conditions that interrupted the deglaciation process and, in some cases, even favored glacier readvances in Europe (31–33).

Our results on the final stages of the last deglaciation illustrate the complexity of the melting of ice sheets that once covered a large fraction of the northern hemisphere continents. Modeling this retreat, together with the associated icebergs and freshwater drainage history, will help in quantifying the complex impact of ice-sheet melting on ocean circulation and, more generally, Earth's climate over the first half of the Holocene period (34, 35). In addition, the observed long-term sea-level changes will allow geophysicists to extract the isostatic “memory” component from modern satellite data to quantify recent processes such as oceanic thermal expansion, melting of mountain glaciers, and loss of ice from the Greenland and West Antarctica ice sheets (36).

## References and Notes

- W. T. Pfeffer, J. T. Harper, S. O'Neel, *Science* **321**, 1340 (2008).
- Materials and methods are available as supporting material on *Science* Online.
- R. G. Fairbanks, *Nature* **342**, 637 (1989).
- E. Bard, M. Arnold, R. G. Fairbanks, B. Hamelin, *Radiocarbon* **35**, 191 (1993).
- R. G. Fairbanks *et al.*, *Quat. Sci. Rev.* **24**, 1781 (2005).
- E. Bard, B. Hamelin, R. G. Fairbanks, A. Zindler, *Nature* **345**, 405 (1990).
- E. Bard, B. Hamelin, R. G. Fairbanks, *Nature* **346**, 456 (1990).
- W. R. Peltier, R. G. Fairbanks, *Quat. Sci. Rev.* **25**, 3322 (2006).
- P. U. Clark, N. G. Pisias, T. F. Stocker, A. J. Weaver, *Nature* **415**, 863 (2002).
- A. J. Weaver, O. A. Saenko, P. U. Clark, J. X. Mitrovica, *Science* **299**, 1709 (2003).
- P. U. Clark, J. X. Mitrovica, G. A. Milne, M. E. Tamisiea, *Science* **295**, 2438 (2002).
- E. Bard *et al.*, *Nature* **382**, 241 (1996).
- S. L. Kanfoush *et al.*, *Science* **288**, 1815 (2000).
- T. Hanebuth, K. Stattegger, P. M. Grootes, *Science* **288**, 1033 (2000).
- J. M. Webster *et al.*, *Geology* **32**, 249 (2004).
- J. D. Stanford *et al.*, *Paleoceanography* **21**, PA4103 (2006).
- P. Deschamps *et al.*, *Geophys. Res. Abstr.* **11**, EGU2009-10233 (2009).
- R. L. Edwards *et al.*, *Science* **260**, 962 (1993).
- I. Shennan, *J. Quat. Sci.* **14**, 715 (1999).
- K. B. Cutler *et al.*, *Earth Planet. Sci. Lett.* **206**, 253 (2003).
- G. Cabioch *et al.*, *Quat. Sci. Rev.* **22**, 1771 (2003).
- S. O. Rasmussen *et al.*, *J. Geophys. Res.* **111** (D6), D06102 (2006).
- L. F. Montaggioni *et al.*, *Geology* **25**, 555 (1997).
- G. Cabioch, G. F. Camoin, L. F. Montaggioni, *Sedimentology* **46**, 985 (1999).
- G. A. Milne, J. X. Mitrovica, *Quat. Sci. Rev.* **27**, 2292 (2008).
- J. X. Mitrovica, N. Gomez, P. U. Clark, *Science* **323**, 753 (2009).
- G. Philippon *et al.*, *Earth Planet. Sci. Lett.* **248**, 750 (2006).
- J. Okuno, M. Nakada, *Palaeogeogr. Palaeoclimatol. Palaeoecol.* **146**, 283 (1999).
- S. E. Bassett, G. A. Milne, J. X. Mitrovica, P. U. Clark, *Science* **309**, 925 (2005).
- F. W. Taylor, P. Mann, *Geology* **19**, 103 (1991).
- B. G. Andersen *et al.*, *Quat. Int.* **28**, 147 (1995).
- J. I. Svendsen, V. Gataullin, J. Mangerud, L. Polyak, *Dev. Quat. Sci.* **26**, 369 (2004).
- V. R. Rinterknecht *et al.*, *Science* **311**, 1449 (2006).
- H. Renssen *et al.*, *Nat. Geosci.* **2**, 411 (2009).
- Z. Liu *et al.*, *Science* **325**, 310 (2009).
- G. A. Milne, W. R. Gehrels, C. W. Hughes, M. E. Tamisiea, *Nat. Geosci.* **2**, 471 (2009).
- The authors thank G. Cabioch for help with coring and sampling; G. Ménot and W. Barthelemy for help with U-Th analyses; D. Borschneck for help with x-ray diffraction analyses; P. Deschamps for age calculations and drafting Fig. 1; P. Dussouillez and J.-J. Motte for help with maps; and F. Antonioli, G. Cabioch, P. Clark, P. Deschamps, and F. Taylor for useful technical and scientific discussions. Numerical data are available in table S1 and also at the National Oceanic and Atmospheric Administration's National Geophysical Data Center public data repository. Paleoclimate work at CEREGE is supported by grants from the Gary Comer Foundation for Science and Education, the European Science Foundation (EuroMARC), the CNRS, and the Collège de France.

## Supporting Online Material

www.sciencemag.org/cgi/content/full/science.1180557/DC1  
SOM Text  
Figs. S1 and S2  
Tables S1 and S2  
References

13 August 2009; accepted 5 January 2010  
Published online 14 January 2010;  
10.1126/science.1180557

Include this information when citing this paper.



[www.sciencemag.org/cgi/content/full/science.1180557/DC1](http://www.sciencemag.org/cgi/content/full/science.1180557/DC1)

## Supporting Online Material for

### **Deglacial Meltwater Pulse 1B and Younger Dryas Sea Levels Revisited with Boreholes at Tahiti**

Edouard Bard,\* Bruno Hamelin, Doriane Delanghe-Sabatier

\*To whom correspondence should be addressed. E-mail: [bard@cerege.fr](mailto:bard@cerege.fr)

Published 14 January 2010 on *Science Express*  
DOI: 10.1126/science.1180557

#### **This PDF file includes:**

SOM Text  
Figs. S1 and S2  
Tables S1 and S2  
References

## **SOM-1/ Scientific context regarding modern and past sea-level changes:**

Recent studies on modern ice sheets suggest that ice-discharge from the Greenland and Antarctica ice-sheets could dominate sea-level changes in the next few centuries (*S1*). However, recording recent sea-level changes is particularly complex because regional variations are often larger than the global average, and high-frequency changes are superimposed on long-term trends that even depend on the memory of pre-existing sea-level over an extended period of time (*S2*).

A complementary way of investigating the behavior of large ice sheets in response to climate change is to study the dramatic sea-level changes that occurred during the last deglaciation. Over such a recent geological period, sufficiently precise markers are available to measure the rate of sea-level change and the retreat of each individual ice sheet, notably the former Laurentide ice sheet (*S2*). Long time series of sea-level data are also crucial for constraining numerical models of glacio-hydro-isostasy (GHI) that are used to correct the post-glacial rebound (PGR) component embedded in recent tide-gauge and satellite data. Furthermore, long sea-level records are of utmost importance as simulation targets for a wide spectrum of numerical models, ranging from three-dimensional thermomechanical ice-sheets (e.g. *S3*) to empirical relationships integrating a multitude of physical responses (e.g. *S4*). The history of deglacial sea-level rise is also crucial as an input for climate models (e.g. *S5*). Indeed, the most sophisticated coupled atmosphere-ocean GCM exhibit a rather linear response to meltwater flux (*S6*) emphasizing the importance of an accurate reconstruction.

Recent studies on modern ice sheets suggest that dynamically forced ice-discharge may already be contributing to the current sea-level rise observed over the last few decades (*S7-S10*). Several dynamic processes have been described in marginal regions, such as enhanced ice flow due to water lubrication of the ice-sheet base (*S11-S13*), loss of buttressing related to ice-shelf break-up, dynamic thinning of the terminus zone of glaciers reaching the ocean (*S14,S15*) and direct melting through contact between the floating ice-tongue and marine waters (*S16*).

However, the large potential impacts of the combination of these dynamic processes has been recognized only recently, which explains why they were just roughly estimated in the most recent IPCC AR4 report (*S17*), but not formally included in numerical models used to simulate the meltwater flux to the ocean. Over the past 17 years, sea-level rose by ca. 3.32 mm/yr (*S18,S19*), partly owing to enhanced ice dynamics superimposed on several other mechanisms such as summer ice ablation, thermosteric and halosteric components, redistribution of water between land and ocean due to human activities. The most recent data since 2003 obtained by satellite altimetry and gravimetry suggest that sea-level rise has been mainly linked to meltwater input to the ocean, whereas thermal expansion was the dominant mechanism during the last decade (*S19*). The complexity of understanding sea-level rise is further illustrated by the difficulty of compiling its local changes and of unraveling its different components. This strongly depends on corrections applied to account for slow post-glacial rebound (PGR) effects, which can be estimated by means of glacio-hydro-isostasy (GHI) models. For example, there are substantial disagreements between recent modeling studies of sea-level and water storage on land and ocean, which could be attributed to differences in the correction used for the PGR component (*S8,S19-S22*).

These geophysical models are tuned to fit the long-term variations of sea-level rise observed at various locations on the planet. During the last glacial maximum (*S23,S24*), the global sea level was about 120-130 m below the present-day level. Glacial ice sheets

subsequently disappeared over a period of 15 kyr known as the last deglaciation. The rate of sea-level change was not constant throughout this period, most notably during episodes of acceleration called Melt Water Pulses (S25-S28).

During both MWP events, the sea-level apparently rose by several meters per century, (i.e. freshwater input to the ocean exceeding 1 Sverdrup =  $10^6$  m<sup>3</sup>/s). This large hydrological perturbation probably impacted the Atlantic meridional overturning circulation (AMOC, S29). MWP events are broadly similar to the so-called Heinrich events that punctuated the last glacial period and caused prominent climatic impacts on a global scale. The amplitude and geographical pattern of these climatic changes have been simulated with numerical models representing the ocean-atmosphere couple (S6,S30-S37). However, the climatic impact is complex because it also depends on whether freshwater remains at the surface before being advected to deep ocean convection zones, or whether the meltwater plume is strongly mixed with sediments and thus entrained onto the seafloor in hyperpycnal flows (S38).

In the same way, there are also some uncertainties in identifying the sources of meltwater and on their routes of injection into the ocean. For MWP-1A around 14 kyr BP, the main debate concerns the relative proportions coming from Antarctica (S39) and the Laurentide ice sheet (S40). Uncertainties also remain about the more recent stages of the deglaciation between 14 and 9 kyr BP, before the final collapse of the residual Laurentide ice sheet and the final drainage of Lake Agassiz. The 14 to 9 kyr BP interval encompasses the prominent Younger Dryas (YD) climatic event, whose immediate and ultimate causes are still mysterious.

Following previous hypotheses (S41,S42), Broecker et al. (S43) reinforced the view that the YD was caused by a diversion of the meltwaters away from a southern route through the Mississippi River system, with the flow being shifted farther east through the Great Lakes and the St. Lawrence River. This view was then criticized based on studies of sediment cores from the mouth of the St. Lawrence estuary (S44). Over the past few years, several authors have acquired new data on land (S45-S48), and in the ocean (S38,S49-S52). A significant result of this research is the recognition of a third, northwestern route, through the McKenzie River outlet directly into the Arctic Ocean (S45,S46). Numerical modeling of the Laurentide ice sheet (S53,S54) even indicated pulses of Arctic discharge coeval with MWP-1A and the onset of YD, but none corresponding to MWP-1B. Nevertheless, the debate on this matter still persists, with active controversy concerning the interpretation of both land (S55-S58) and ocean records (S59-S61).

## **SOM-2/ Background information on deglacial sea-level reconstructions:**

In this section, we describe the sea-level records and provide a specific background on their particular strengths and pitfalls. Reef-building corals are widely used as sea-level indicators, due to their symbiosis with zooxanthellae, which need light for their photosynthesis. The biodiversity in Caribbean reefs is rather low and the reef crests are occupied by the dominant species *Acropora palmata*, which forms monospecific frameworks at shallow depth. By contrast, a more diverse biological association is observed in the Indo-Pacific province, including branching corals and encrusting coralline algae.

Another complication inherent to all coral records is linked to correcting for vertical movements. The correction is generally simplified as a constant vertical rate, specific to each drill site. This approximation may not always be valid for sites located in subduction zones. Indeed, vertical movements result from episodic coseismic uplift, with individual steps of the

order of a few meters lifting up the coral reef (S62). Therefore, the assumption of constant uplift may not apply to short timescales, and might lead to some scatter of the data. By contrast, Tahiti was formed by a hot-spot volcano, which is now slowly subsiding in the middle of the Pacific plate. The absence of abrupt changes in vertical movement is a particular strength of the Tahiti record.

### Central Pacific

We previously used Thermal Ionization Mass Spectrometry (TIMS) to date a suite of corals sampled in two vertical cores from the outer barrier reef flat of Papeete harbor at Tahiti (S63). The short P6 core (50 m) only covers the past 10 kyr BP, but the other core (P7) successfully penetrated the whole Holocene and Late-Glacial sequence, before reaching an older and recrystallized level at 87 m making up the pre-LGM reef, and, at greater depth, the volcanic substratum (114 m below present sea level, b.p.s.l).

Although core P7 provides a continuous record over the MWP-1B interval, the precise structure of the sea-level curve remains unclear, with only two coral samples in the critical interval. This provided the justification for drilling a series of new long cores in the same Papeete Barrier reef by means of the IRD drilling rig (Sedidril). In an attempt to reach the outer layers of the reef, the new cores were drilled with deviations from the vertical.

Figure S1 shows a map of the Papeete barrier reef and lagoon. The P8 core was deviated at an angle of 33° towards the sea on the outer reef flat, while P9 and P10 were drilled in the inner part of the barrier reef. These cores were drilled on the edge of the Papeete Pass, with a deviation of 30° towards the pass (i.e. parallel to the barrier for P9). All depths given here (Table S1) are converted to a vertical scale (see S64, S65 for details of the logistic aspects and a description of the cored material).

As described previously (S63), our sea-level reconstruction is based on a biological assemblage typical of the immediate subsurface habitat in Polynesia. Systematic observations, including direct investigation at Tahiti (S63, S66 and references therein) have shown that the reef front is composed of widespread colonies of branching *Acropora* and *Pocillopora* locally capped by carbonate crusts of the coralline red algae *Hydrolithon onkodes*. This algo-coral assemblage disappears below about 6 m water depth and is replaced by a community tolerant to deeper conditions, including corals such as *Porites* and *Favidea*.

Because of their relative positions with respect to the barrier reef (map in Fig. S1), we should also expect differences between the biological associations recovered in the different drill cores. As predicted by numerical modeling of reef growth (Fig. 3 in S63 and further tests with the same model), the lower part of core P8 sampled material from the outer-reef slope (numerous *Porites* samples were dated below 65 m in the P8 core; see Table S1). As shown in Fig. 1b, the depth difference of these deeper P8 samples with those found in other cores is quite systematic. Nevertheless, it remains limited to about 6 m, within the bathymetric range of the most restricted coral species (this may explain the presence of three isolated *Acropora* and *Pocillopora* samples among a majority of *Porites* samples). In any case, corals found below 65 m in the P8 core should be excluded to estimate average rates of sea-level rise (see more details below about these calculations).

In addition, the biological associations in cores P9 and P10 are probably affected by the lagoon outlet (present width and depth are 110 m and 12 m, respectively). This so-called Papeete Pass is a morphological feature linked to the Tipaerui River (see map in Fig. S1). When sea level was lower during the deglaciation, the Tipaerui River discharged its load of

freshwater and terrigenous material directly at the Papeete Pass. An increase in water turbidity is compatible with higher concentrations of terrigenous sand in the lower part of the P9 and P10 cores (S64), which could thus explain the relative abundance of *Porites* colonies in the lower core sections, and the relative scarcity of branching corals (*Acropora* and *Pocillopora*).

Tahiti is an island formed by a hot-spot volcano, characterized by a slow and regular subsidence estimated at about 0.25 mm/yr. This value is based on the literature (S67,S68) and on K-Ar dating of a sub-aerial lava flow sampled at the bottom of core P7 (S63). This uplift rate translates to a systematic upward correction of ca. 2-3 m in the time window of interest for this paper. Assuming an error of  $\pm 0.2$  mm/yr would lead to a difference of a  $\pm 2$  meters at the time of MWP-1B. Such an uncertainty on the uplift correction is well within the paleo-bathymetric uncertainty corresponding to the living-depth range of the corals.

Table S1 lists the new U-Th data measured on coral samples from cores P8, P9 and P10 forming the basis of this study. Two thirds of the U-Th ages were measured on samples of *Acropora* and *Pocillopora*, which strengthens the sea-level reconstruction for Tahiti. In-place coral colonies can be recognized unambiguously in the cores, from the upward position of the tips of branching corals and the coralline coatings. All coral samples were first checked for the absence of secondary calcite, using X-ray diffraction (XRD, S69), and processed via the same U-Th techniques as reported previously (S63,S70). Isotopic ratios and ages were calculated using revised  $^{234}\text{U}$  and  $^{230}\text{Th}$  half-lives (S71). The initial  $^{234}\text{U}/^{238}\text{U}$  ratio ( $\delta^{234}\text{U}_i$ ) values range between 142 and 150 ‰ (Table S1), with an average value of 146.8 ‰ and a standard deviation of 1.8‰ (n=50). These values are in good agreement with previous analyses in cores P6 and P7 (Table S1, average value of 144.6 ‰, st. dev. of 1.4‰, n=34). For all Tahiti samples in Table S1, the average  $\delta^{234}\text{U}_i$  is 145.9 ‰ with a standard deviation of 2.0 ‰ (n=84). This is similar to  $\delta^{234}\text{U}$  measured on modern and recent corals at CEREGE (S72) as well as by other teams (e.g. S71,S73). The Tahiti  $\delta^{234}\text{U}_i$  values are in the range proposed as a reliability criterion (S74), thus confirming the visual inspection and XRD analyses of the samples.

The results listed in Table S1 are represented graphically on Figure 1 by plotting depth, corrected for subsidence, versus U-Th ages. To estimate average rates of sea-level rise with their standard errors, linear fits are calculated for the entire period of interest (9-14 kyr BP) and for specific time intervals related to known climatic boundaries (before, during and after the YD event as defined from climatic boundaries well dated in the Greenland NorthGRIP ice core: 12,850 and 11,650 cal-yr-BP for the YD start and end, respectively, S75).

Over the entire 9-14 kyr BP period, the average sea-level rise is  $10.2 \pm 0.2$  mm/yr ( $R^2=0.98$ ). Interestingly, the linear fit remains extremely similar (slope of  $10.3 \pm 0.2$  mm/yr,  $R^2=0.98$ ) by excluding the 24 samples made of *Porites* and *Favidea* (triangles in Fig. 1b). Over the specific time intervals related to the YD event, the sea-level rise rates are the following:  $10.9 \pm 1.0$  mm/yr ( $R^2=0.90$ );  $9.9 \pm 1.4$  mm/yr ( $R^2=0.80$ );  $11.7 \pm 0.4$  mm/yr ( $R^2=0.96$ ) for the periods before, during and after the YD event, respectively. These rates can also be calculated by excluding samples made of *Porites* and *Favidea* (triangles in Fig. 1b):  $12.1 \pm 0.6$  mm/yr ( $R^2=0.99$ );  $7.5 \pm 1.1$  mm/yr ( $R^2=0.96$ );  $11.7 \pm 0.4$  mm/yr ( $R^2=0.96$ ) for the periods before, during and after the YD event, respectively. We consider these latter values as best estimates, which are plotted as grey bars in Figure 1b. The rate during the YD ( $7.5 \pm 1.1$  mm/yr) is statistically different from those calculated for the entire 9-14 kyr period ( $10.3 \pm 0.2$  mm/yr), and periods before and after the YD. The latter is characterized by a sea-level rise rate ( $11.7 \pm 0.4$  mm/yr) significantly larger than for the entire 9-14 kyr period ( $10.3 \pm 0.2$  mm/yr). These conclusions would remain unchanged even if samples below 65 m in core P8 were included in

the calculations:  $12.4 \pm 1.1$  mm/yr ( $R^2=0.96$ );  $6.0 \pm 3.6$  mm/yr ( $R^2=0.48$ );  $11.7 \pm 0.4$  mm/yr ( $R^2=0.96$ ) for the periods before, during and after the YD event, respectively, and  $10.4 \pm 0.2$  mm/yr ( $R^2=0.98$ ) for the entire period.

Results of the linear fit calculations are summarized in Table S2, showing that our preferred solution (only *Acropora* and *Pocillopora* samples, dots in Fig. 1b, exclusion of P8 samples below 65 m) also leads to the highest  $R^2$  and most precise determinations of sea-level rates.

### Caribbean Sea

Fairbanks et al. (S76) published replicate U-Th ages measured by Multi-Collector Inductively Coupled Mass Spectrometry (MC-ICPMS), obtained from the same suite of corals previously dated by TIMS by Bard et al. (S26,S27). As expected, the recent data are often slightly more precise than the previous results measured with an older generation mass spectrometer (VG MM30). However, both datasets are compatible within errors if we take into account the revised  $^{234}\text{U}$  and  $^{230}\text{Th}$  half-lives (S71) and a known bias of the  $^{234}\text{U}/^{238}\text{U}$  linked to the limited abundance sensitivity of instruments used in the 1980s (see S70 for evidence of this small bias and S72 for a comparison, based on U standards, with measurements performed on the modern TIMS facility used at CEREGE to analyze the Tahiti corals).

The Barbados reef crest is dominated by the coral species *Acropora palmata*, which is generally considered as representative of water depths less than 5 m, although it has been reported as living occasionally at greater depths, down to 17 m (S77). In addition to the *A. palmata* samples, the Barbados database was augmented (S28) by reporting U-Th ages measured on other corals such as *Montastrea annularis*, *Porites asteroides* and *Diploria*, which live systematically below the reef crest in the Caribbean. As assumed by Peltier & Fairbanks (S28), the living depth range of these corals is about 20 m for *M. annularis* and about 50 m for the other two species. Therefore, these additional data are of little help in constraining sea-level changes during MWP-1B, so we prefer to continue using the U-Th results measured on *A. palmata* samples, following Fairbanks (S25) and Bard et al. (S26,S27).

The Barbados sea-level curve is based on three reef cores drilled off the southwestern coast of the island (S25). MWP-1B corresponds to the gap between sample RGF7-27-4, dated at  $11,080 \pm 75$  cal-yr-BP at the bottom of core #7 (41 m recovery depth below present sea level b.p.s.l), and RGF12-5-2, dated at  $11,390 \pm 45$  cal-yr-BP at the top of core #12 (53 m b.p.s.l). The age and depth of this coral is confirmed by the results from sample RGF12-6-7 ( $11,510 \pm 75$  cal-yr-BP at 55 m b.p.s.l) in the same core, as well as by two additional *A. palmata* samples dated in the nearby core #16 (RGF16-12-6 and RGF16-12-7 at 54 m b.p.s.l and dated at  $11,510 \pm 35$  and  $11,390 \pm 70$  cal-yr-BP, respectively). These MC-ICPMS U-Th ages (S28) are compatible with those previously measured by TIMS (S26,S27), yielding ages of  $11,075 \pm 70$ ,  $11,570 \pm 60$ , and  $11,510 \pm 70$  cal-yr-BP for samples RGF7-27-4, RGF12-5-2 and RGF12-6-7, respectively.

The island of Barbados is located on the accretionary prism at the convergent boundary between the Caribbean and South American plates, at an intermediate distance from the former Laurentide Ice Sheet. As for previous studies (S25-S27), the sample depths are corrected for a long-term tectonic uplift of 0.35 mm/yr. This value is the average between the uplift rates derived from the elevation of the last interglacial terrace (Rendezvous Hill) on the southwest and west coasts of Barbados (30 and 60 m, respectively). Due to this tilt of the island, the

southwest transect (Christ-Church area) shows an uplift rate of 0.25 mm/yr and the west transect (Clermont-Nose) about 0.45 mm/yr (S78,S79).

The results obtained on *A. palmata* samples are presented graphically on Figure 1d by plotting depth corrected for uplift versus the U-Th ages (S28). As for the Tahiti record, we calculate linear fits for the entire period and specific time intervals.

Over the entire 9-14 kyr BP period, the average sea-level rise is  $10.5 \pm 0.5$  mm/yr ( $R^2=0.96$ ) similar to that calculated for Tahiti ( $10.3 \pm 0.2$  mm/yr,  $R^2=0.98$ ). For Barbados, the sea-level rise rates are  $9.3 \pm 0.4$  mm/yr ( $R^2=0.99$ ) before the YD and  $5.5 \pm 0.9$  mm/yr ( $R^2=0.90$ ) during the YD.

In the Barbados record, five samples were recovered from core #12 within the YD chronozone. They are well aligned in Fig. 1d, and define a rate of rise of  $5.5 \pm 0.9$  mm/yr ( $R^2=0.93$ ). Moreover four other samples were dated around 11.5 kyr BP in cores #12 and #16, evidently aligned with those in the YD interval. Indeed, grouping these 4 samples with those belonging to the YD, leads to a rate of  $5.6 \pm 0.4$  mm/yr ( $R^2=0.97$ ), similar to that calculated for the YD *stricto sensu*. The original MWP-1B corresponds to the gap between cores #12 and #7 and the two extreme samples lead to a rate of 40 mm/yr. All samples from the upper core (#7) are well aligned, defining a rate of  $8.4 \pm 0.6$  mm/yr ( $R^2=0.96$ ) during the early Holocene, a value significantly higher than the one observed for the YD.

A precise examination of the position of these cores along the coast of Barbados shows that core #7 is relatively far from Oistins Bay where the other cores were drilled (see precise bathymetric map in Fig. S2b). Indeed, cores #12 and #16 were drilled in a submerged morphologic feature equivalent to the relict reef studied by means of a submersible (S80). By contrast, Core #7 is located on the fringing reef off Kendal Point and South Point. A systematic bathymetric difference between both environments could be invoked, but this hypothesis would imply that, during the sea-level transition, the depth tolerance of *A. palmata* exceeded its 5 m limit, observed during the modern period characterized by sea-level stability (similar to the “no-analog” problem of transfer functions based on microfossils). We note that Goreau (S77) observed modern living *A. palmata* at a depth of 17 m.

As summarized by Taylor & Mann (S81), Barbados is not only characterized by a general uplift of varying amplitude around the island, but also exhibits several faults and tectonic flexures (see map in Fig. S2a). As mentioned above, MWP-1B is bracketed by samples recovered from cores #12 and #7 drilled at 41 and 10 m below present sea level, respectively. Therefore, it is possible that these cores belong to different tectonic segments, separated by the offshore prolongation of a tectonic structure previously mapped on the island (S81). In this case, core #7 could thus be affected by a higher uplift rate than the other cores used for the Barbados sea-level reconstruction. Additional geological and geophysical data for Barbados are needed to settle this issue. However, it remains unlikely that a tectonic bias could explain the full amplitude of the MWP-1B step (15-m). Even tripling the uplift rate of the Barbados south coast from 0.35 mm/yr to 1 mm/yr would account for only half the observed amplitude of MWP-1B. Such a bias in uplift rate (0.65 mm/yr) is not detectable by looking at the difference between the average rates of sea-level rise calculated for Barbados and Tahiti ( $10.5 \pm 0.5$  and  $10.3 \pm 0.2$  mm/yr, respectively). In other words, the uncertainties on these rates do not allow supporting or ruling out such a hypothesis.

### **West Pacific**

Edwards et al. (S82) obtained U-Th ages on a 52 m-long core collected in the post-glacial fringing reef complex at Kwambu, Huon Peninsula, Papua New Guinea. This dataset had been compared with the published Tahiti record based on cores P6 and P7 (S63). Two additional corals were then added from this core in the time window of interest (S83, blue dots in Fig. 1c). The Huon Peninsula is characterized by a high uplift rate in relation to the subduction zone between the Australia and Pacific plates. The vertical uplift rate varies between 1 and 4 mm/yr along the coastline, with an average of about 1.9 mm/yr estimated for the drilling site at Kwambu (S84). The rate is assumed as constant to correct the recovery depths of the dated coral samples.

Over the entire 9-14 kyr BP period, the average sea-level rise is  $9.4 \pm 0.8$  mm/yr ( $R^2=0.92$ ), statistically undistinguishable from those calculated for Tahiti ( $10.3 \pm 0.2$  mm/yr) and Barbados ( $10.5 \pm 0.5$  mm/yr). At Huon, the sea-level rise rates are  $10.4 \pm 1.7$  mm/yr ( $R^2=0.91$ ) within the YD and  $15.6 \pm 1.7$  mm/yr ( $R^2=0.95$ ) during the early Holocene.

The specific problem of the Huon record is its data gap between 12.1 and 11.1 kyr BP, encompassing the second half of the YD event and the MWP-1B period defined at Barbados. A rather low sea-level rate (5.7 mm/yr) is calculated by using the two samples bracketing the data gap. However, this problem makes it difficult to compare with the Tahiti and Barbados record. In any case, the sea-level rise is slower during the YD than during the early Holocene, in agreement with records from other sites.

Cabioch et al. (S85) presented results obtained on a transect of cores collected at Urélapa, Vanuatu, located at the convergent boundary of the Australia and Pacific plates. This island is characterized by a very high uplift rate, of the order of 3 mm/yr, explaining why the entire deglaciation is compressed into about 40 m (i.e. one third of its original amplitude). In the time window of interest, the Vanuatu record only includes seven samples from two different cores, which are plotted in Fig. 1c in comparison with the Huon record. However, we cannot calculate reliable rates of sea-level change based on so few data points.

Finally, the Sunda shelf record, based on  $^{14}\text{C}$  dating of shoreline indicators (S86), is not included in this discussion, since only two samples were collected between 13 and 9 kyr BP, which is insufficient for the study of MWP-1B. In addition, the calibration of  $^{14}\text{C}$  ages makes it inherently less precise than sea-level records based on U-Th dating, which directly provides calendar ages.

### Supplementary References :

- S1. W. T. Pfeffer, J. T. Harper, S. O'Neel, *Science* **321**, 1340 (2008).
- S2. G. A. Milne *et al.*, *Nat. Geosci.* **2**, 471 (2009).
- S3. M. J. R. Simpson, G. A. Milne, P. Huybrechts, A. J. Long, *Quat. Sci. Rev.* **28**, 1631 (2009).
- S4. M. Siddall, T. F. Stocker, P. U. Clark, *Nat. Geosci.* **2**, 571 (2009).
- S5. H. Renssen *et al.*, *Nat. Geosci.* **2**, 411 (2009).
- S6. Z. Liu *et al.*, *Science* **325**, 310 (2009).
- S7. I. Velicogna, J. Wahr, *Science* **311**, 1754 (2006).
- S8. M. van den Broeke, *Science* **326**, 984 (2009).
- S9. E. Rignot *et al.*, *Nat. Geosci.* **1**, 106 (2008).
- S10. E. Rignot, J. E. Box, E. Burgess, E. Hanna. *Geophys. Res. Lett.* **35**, L20502 (2008).
- S11. H. J. Zwally *et al.*, *Science* **297**, 218 (2002).
- S12. I. Joughin *et al.*, *Science* **320**, 781 (2008).
- S13. S. Das *et al.*, *Science* **320**, 778 (2008).
- S14. A. Sole *et al.*, *Cryosphere Discuss.* **2**, 673 (2008).
- S15. I. M. Howat, I. Joughin, T. A. Scambos, *Science* **315**, 1559 (2007).
- S16. D. M. Holland *et al.*, *Nat. Geosci.* **1**, 659 (2008).
- S17. S. D. Solomon, M. Manning, D. Qin (eds) *Climate Change 2007: The Physical Basis 4<sup>th</sup> Assessment Report, IPCC 18* (Cambridge Univ. Press, Cambridge, 2007).
- S18. J. A. Church, N. J. White, *Geophys. Res. Lett.* **33**, L01602 (2006).
- S19. A. Cazenave *et al.*, *Glob. Planet. Change* **65**, 83 (2009).
- S20. V. R. Barletta, R. Sabadini, A. Bordoni, *Geophys. J. Int.* **172**, 18 (2008).
- S21. J. K. Willis, D. T. Chambers, R. S. Nerem, *J. Geophys. Res.* **113**, C06015 (2008).
- S22. W. R. Peltier, *Quat. Sci. Rev.* **28**, 1658 (2009).
- S23. A. C. Mix, E. Bard, R. Schneider, *Quat. Sci. Rev.* **20**, 627 (2001).
- S24. P. U. Clark *et al.*, *Science* **325**, 710 (2009).
- S25. R. G. Fairbanks, *Nature* **342**, 637 (1989)
- S26. E. Bard, B. Hamelin, R. G. Fairbanks, A. Zindler, *Nature* **345**, 405 (1990).
- S27. E. Bard, B. Hamelin, R. G. Fairbanks, *Nature* **346**, 456 (1990).
- S28. W. R. Peltier, R. G. Fairbanks, *Quat. Sci. Rev.* **25**, 3322 (2006).
- S29. P. U. Clark, N. G. Pisias, T. F. Stocker, A. J. Weaver, *Nature* **415**, 863 (2002).
- S30. A. J. Weaver, O. A. Saenko, P. U. Clark, J. X. Mitrovica, *Science* **299**, 1709 (2003).
- S31. S. Manabe, R. J. Stouffer, *Nature* **378**, 165 (1995).
- S32. S. Manabe, R. J. Stouffer, *Quat. Sci. Rev.* **19**, 285 (2000).
- S33. A. Ganopolski, S. Rahmstorf, *Nature* **409**, 153 (2001).
- S34. D. Seidov, R. J. Stouffer, B. J. Haupt, *Glob. Planet. Change* **49**, 19 (2005).
- S35. R. J. Stouffer, D. Seidov, B. J. Haupt, *J. Clim.* **20**, 436 (2007).
- S36. J. Trevena, W. P. Sijp, M. H., *Geophys Res Lett* **35**, L09704 (2008).
- S37. D. Swingedouw, T. Fichefet, H. Goosse, M. F. Loutre, *Clim. Dyn.* **33**, 365 (2009).
- S38. P. Aharon, *Earth Planet. Sci. Lett.* **241**, 260 (2006).
- S39. P. U. Clark, J. X. Mitrovica, G. A. Milne, M. E. Tamisiea. *Science* **295**, 2438 (2002).
- S40. W. R. Peltier, *Quat. Sci. Rev.* **24**, 1571 (2005).
- S41. R. G. Johnson, B. T. McClure, *Quat. Res.* **6**, 325 (1976).
- S42. C. Rooth. *Prog Oceanogr.* **11**, **131** (1982).
- S43. W. S. Broecker *et al.*, *Nature* **341**, 318 (1989).

- S44. A. de Vernal, C. Hillaire-Marcel, G. Bilodeau, *Nature* **381**, 774 (1996).
- S45. J. T. Teller, D. W. Leverington, J. D. Mann, *Quat. Sci. Rev.* **21**, 879 (2002).
- S46. J. T. Teller *et al.*, *Quat. Sci. Rev.* **24**, 1890 (2005).
- S47. J. P. Donnelly *et al.*, *Geology* **33**, 89 (2005).
- S48. T. V. Lowell *et al.*, *Quat. Sci. Rev.* **28**, 1597 (2009).
- S49. B. P. Flower, D. W. Hastings, H. W. Hill, T. M. Quinn, *Geology* **32**, 597 (2004).
- S50. A. E. Carlson *et al.*, *Proc. Nat. Acad. Sci.* **104**, 6556 (2007).
- S51. A. E. Carlson, J. S. Stoner, J. P. Donnelly, C. Hillaire-Marcel, *Geology* **36**, 359 (2008).
- S52. A. E. Carlson *et al.*, *Nat. Geosci.* **1**, 620 (2008).
- S53. L. Tarasov, W. R. Peltier, *Nature* **435**, 662 (2005).
- S54. L. Tarasov, W. R. Peltier, *Quat. Sci. Rev.* **25**, 659 (2006).
- S55. T. G. Fisher, T. V. Lowell, H. M. Loope, *Quat. Sci. Rev.* **25**, 1137 (2006).
- S56. J. T. Teller, M. Boyd, *Quat. Sci. Rev.* **25**, 1142 (2006).
- S57. A. E. Carlson, P. U. Clark, S. W. Hostetler, *Quat. Sci. Rev.* **28**, 2546 (2009).
- S58. T. V. Lowell, T. G. Fisher, *Quat. Sci. Rev.* **28**, 2548 (2009).
- S59. W. R. Peltier *Geology* **35**, 1147 (2007).
- S60. A. E. Carlson, P. U. Clark, *Geology* **36**, e177 (2008).
- S61. W. R. Peltier, A. de Vernal, C. Hillaire-Marcel, *Geology* **36**, e178 (2008).
- S62. J. M. Pandolfi, M. M. R. Best, S. P. Murray, *Geology* **22**, 239 (1994).
- S63. E. Bard *et al.*, *Nature* **382**, 241 (1996).
- S64. G. Cabioch, G. F. Camoin, L. F. Montaggioni, *Sedimentology* **46**, 985 (1999).
- S65. G. Cabioch, Y. Join, C. Ihilly, J. L. Laurent, *Rapp. Missions ORSTOM* **32**, pp. 15, (1995).
- S66. G. Cabioch, L. F. Montaggioni, G. Faure, A. Ribaud, *Quat. Sci. Rev.* **18**, 1681 (1999).
- S67. P. A. Pirazzoli, L. F. Montaggioni, *Palaeogeogr., Palaeoclim., Palaeoecol.*, **68**, 153 (1988).
- S68. I. Le Roy, Ph. D. Thesis, University of Paris XI, pp. 271, (1994).
- S69. S. Sépulcre, N. Durand, E. Bard, *Glob. Planet. Change* **66**, 1 (2009).
- S70. E. Bard *et al.*, *Nucl. Inst. Meth. B-* **52**, 461 (1990).
- S71. H. Cheng *et al.*, *Chem. Geol.* **169**, 17 (2000).
- S72. D. Delanghe, E. Bard, B. Hamelin, *Mar. Chem.* **80**, 79 (2002).
- S73. M. B. Andersen *et al.*, *Earth Planet. Sci. Lett.* **259**, 171 (2007).
- S74. K. A. Hughen *et al.*, *Radiocarbon* **46**, 1059 (2004).
- S75. S. O. Rasmussen *et al.*, *J. Geophys. Res.* **111**, D06102 (2006).
- S76. R. G. Fairbanks *et al.*, *Quat. Sci. Rev.* **24**, 1781 (2005).
- S77. T. F. Goreau, J. W. Wells, *Bull. Mar. Sci.* **17**, 442 (1967).
- S78. R. K. Matthews, *Quat. Res.* **3**, 147 (1973).
- S79. M. L. Bender *et al.*, *Geol. Soc. Am. Bull.* **90**, 577 (1979).
- S80. I. G. Macintyre *et al.*, *Coral Reefs* **10**, 167 (1991).
- S81. F. W. Taylor, P. Mann, *Geology* **19**, 103 (1991).
- S82. R. L. Edwards *et al.*, *Science* **260**, 962 (1993).
- S83. K. B. Cutler *et al.*, *Earth Planet. Sci. Lett.* **206**, 253 (2003).
- S84. Y. Ota, J. Chappell, *Quat. Int.* **55**, 51 (1999).
- S85. G. Cabioch *et al.*, *Quat. Sci. Rev.* **22**, 1771 (2003).
- S86. T. Hanebuth, K. Stattegger, P. M. Grootes, *Science* **288**, 1033 (2000).
- S87. H. Bösscher, W. Schlager, *Sedimentology* **39**, 503 (1992).

### Supplementary Figure 1 (Fig. S1):

Schematic map of the Papeete harbor in Tahiti showing the locations of drill-holes in the barrier reef (S64-S65): vertical cores (P6 and P7 dated previously, S63) and the three deviated cores used for the present study. Black arrows show the drilling orientation (towards the open ocean for P8, towards the pass for P9 and P10).

### Supplementary Figure 2 (Fig. S2):

**Left panel:** Structural map of Barbados taken from Taylor & Mann (S81). Thick lines show the major faults or structural fronts (tick on downthrown side).

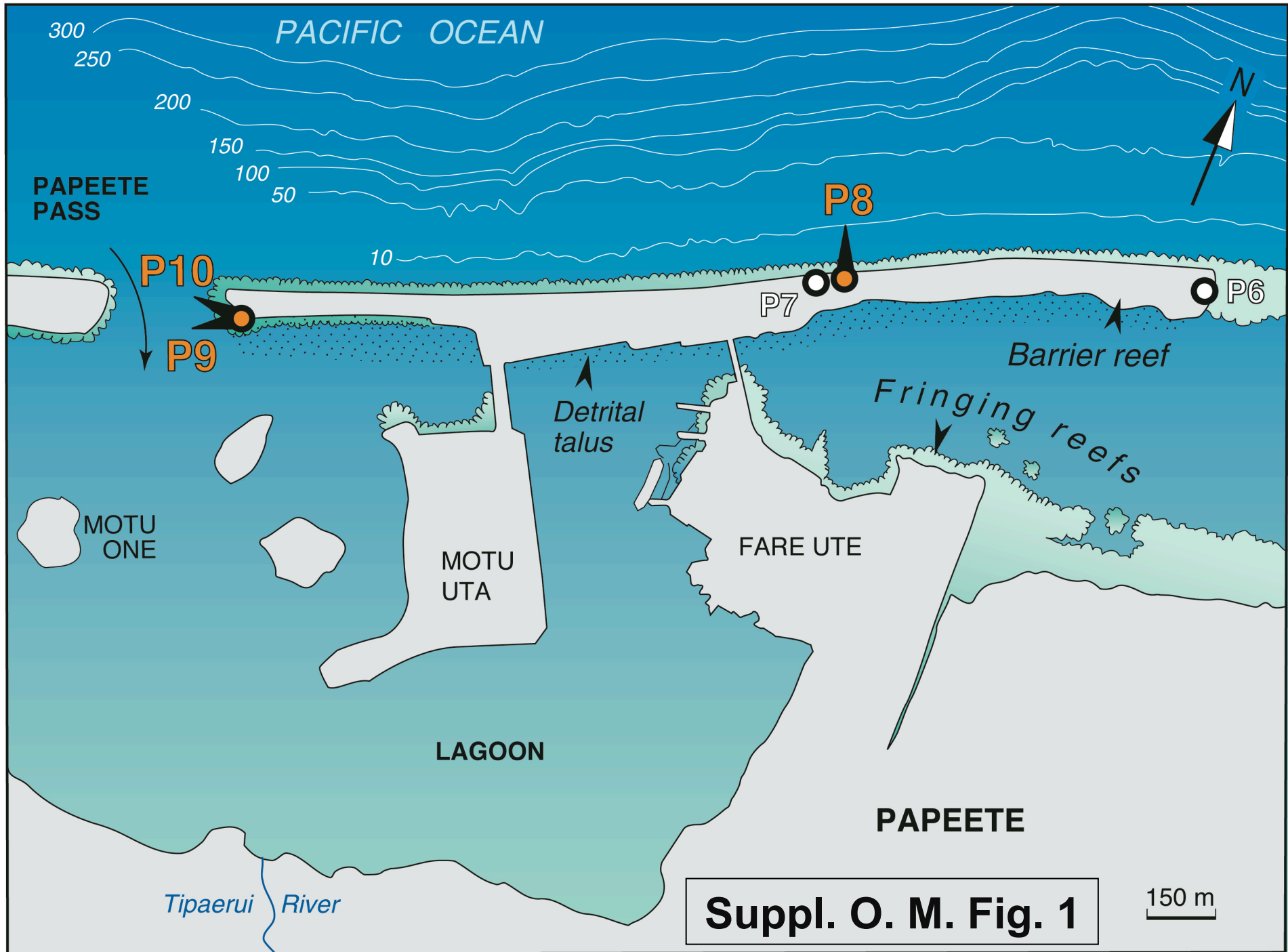
**Right panel:** Bathymetric map (zoom of the square in left panel) showing the area drilled to recover the Barbados core collection (SHOM, Service Hydrographique et Océanographique de la Marine, French Ministry of Defence). The dotted lines (red and white) underline the possible extension of a tectonic structure affecting the south coast (see main text and SOM-2).

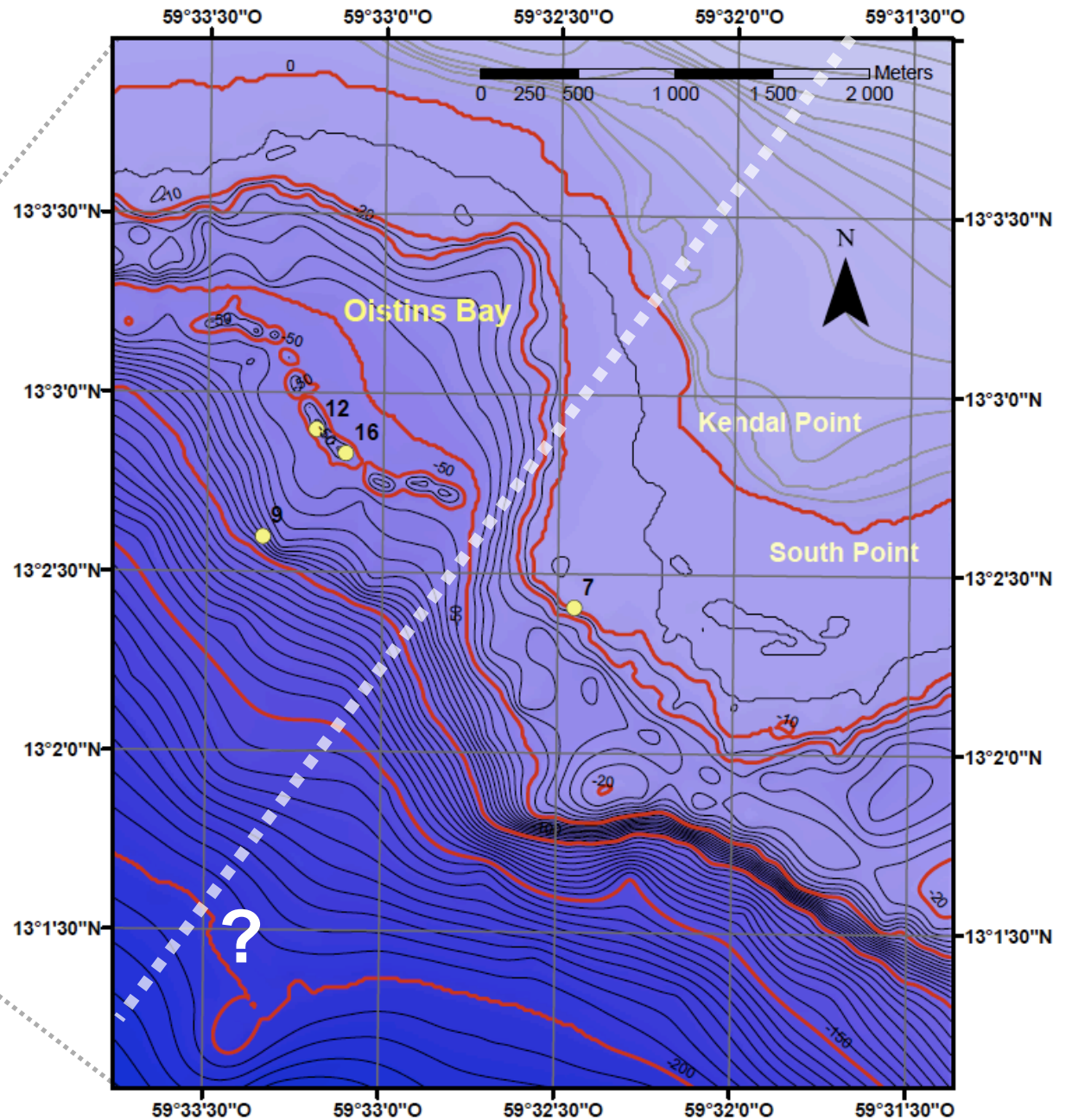
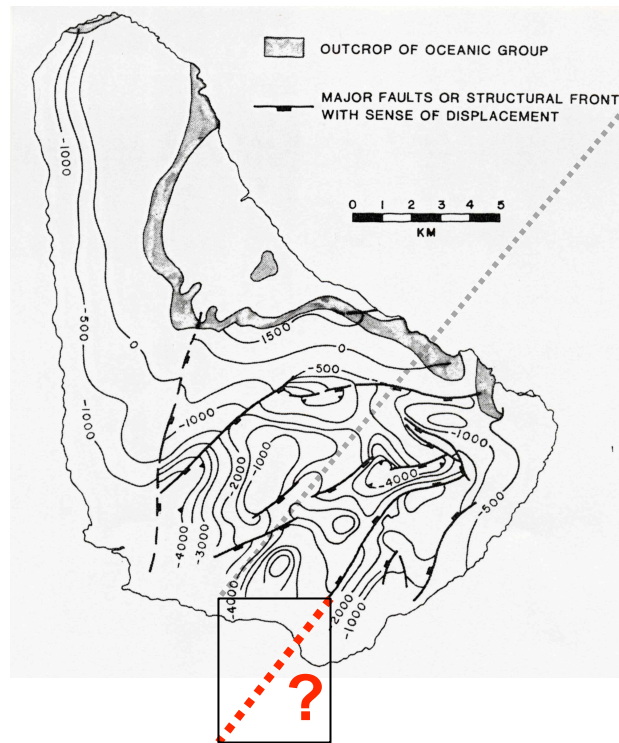
### Supplementary Table S1:

U-Th ages for Tahiti corals (before year A.D. 1950). Results on corals from cores P6 and P7 were reported previously (S63). The new results are those from cores P8, P9 and P10 (see text in SOM-2). The recovery depth is in meters below the present sea level. Labels #1, #2, etc, stand for replicated analyses obtained on different pieces of the same coral sample. Absence of secondary calcite has been checked by XRD (S69). The measured atomic ratios have been converted to activity ratios by using the revised U-Th decay constants (S71). All errors on isotopic ratios are given at the 2 sigma level. The precision of U-content measurements is about 2%. More details on our mass spectrometric techniques can be found in previous publications (S63,S70,S72). The third column provides the species and/or genus of the dated corals. The bathymetric habitat of *Acropora* with *Pocillopora* is more restricted (about 6 m) than those of *Porites* or *Favidea* corals, which can live in the top 10-20 m. In any case, the reliability of biological paleobathymetric indicators is always a statistical notion that should be verified by looking at the scatter among samples in the same core section. This is the reason why we only show two representative ranges in Fig. 1. In principle, these errors should be asymmetric and represented by a probability distribution based on modern observations of occurrence or a physiological law mimicking the observations (S87).

### Supplementary Table S2:

Values of the slopes and standard errors in mm/yr, and  $R^2$  of the linear fits calculated for the different sea-level records corrected for tectonic uplift (see discussion in SOM-2). The different columns correspond to the time intervals related to the YD event boundaries. For Tahiti, the high sample number allows making different calculations by excluding or including samples from the base of P8, and samples made of *Porites* and *Favidea* corals (triangles in Fig 1b, see also Table S1). For Barbados, the two very similar slopes provided for the YD chronozone correspond to calculations including or excluding the 4 samples dated around 11.5 kyr BP in cores #12 and #16 (see discussion in SOM-2). Bold numbers in Table S2 correspond to the linear fits shown in Fig. 1. Those represented as dashed lines for New Guinea correspond to the millennium-long gap starting in the middle of the YD and to the period before YD based on two data points only.





**Suppl. O. M. Fig. 2**

SAMPLE	DEPTH (m)	CORAL SPECIES	<sup>238</sup> U ppm	<sup>230</sup> Th/ <sup>238</sup> U ±2σ	<sup>234</sup> U/ <sup>238</sup> U ±2σ	U-Th age (yr BP) ±2σ	δ <sup>234</sup> U (‰) ±2σ
Ta-P6-10#1	37.5	<i>Acropora danai</i>	3.43	0.09699	0.00041	1.1417 0.002	<b>9632</b> 47 145.6 2
Ta-P6-10#2	37.5	<i>Acropora danai</i>	3.40	0.09715	0.00039	1.1410 0.002	<b>9656</b> 45 144.9 2
Ta-P6-10#3	37.5	<i>Acropora danai</i>	3.32	0.09673	0.00030	1.1425 0.002	<b>9599</b> 36 146.4 3
Ta-P6-11#1	40.3	<i>Acropora danai</i>	3.31	0.09954	0.00039	1.1421 0.002	<b>9895</b> 46 146.1 2
Ta-P6-11#2	40.3	<i>Acropora danai</i>	3.42	0.09927	0.00053	1.1404 0.003	<b>9883</b> 62 144.4 2
Ta-P6-12	42.6	<i>Acropora sp</i>	3.05	0.10031	0.00040	1.1418 0.002	<b>9978</b> 47 145.8 2
Ta-P6-13#1	47.0	<i>Acropora danai</i>	3.67	0.10257	0.00050	1.1415 0.002	<b>10218</b> 56 145.6 3
Ta-P6-13#2	47.0	<i>Acropora danai</i>	3.64	0.10319	0.00039	1.1408 0.002	<b>10289</b> 46 144.9 2
Ta-P6-14#1	49.0	<i>Acropora danai</i>	3.79	0.10214	0.00055	1.1405 0.003	<b>10182</b> 66 144.6 2
Ta-P7-2#1	35.1	<i>Montastrea annuligera</i>	2.43	0.09364	0.00056	1.1358 0.004	<b>9336</b> 68 139.4 4
Ta-P7-2#2	35.1	<i>Montastrea annuligera</i>	2.42	0.09374	0.00041	1.1412 0.003	<b>9299</b> 49 144.9 3
Ta-P7-4	47.1	<i>A. gpe robusta/danai</i>	3.81	0.10327	0.00040	1.1391 0.002	<b>10314</b> 47 143.2 2
Ta-P7-5	50.0	<i>P. cf verrucosa</i>	2.80	0.10628	0.00052	1.1383 0.003	<b>10638</b> 61 142.5 3
Ta-P7-6	56.0	<i>Favidea</i>	2.73	0.10909	0.00054	1.1403 0.003	<b>10914</b> 65 144.7 3
Ta-P7-7#1	56.1	<i>Acropora sp</i>	3.89	0.11045	0.00040	1.1402 0.002	<b>11059</b> 48 144.6 2
Ta-P7-7#2	56.1	<i>Acropora sp</i>	3.99	0.11076	0.00031	1.1420 0.002	<b>11073</b> 39 146.5 2
Ta-P7-7#3	56.1	<i>Acropora sp</i>	3.84	0.11071	0.00033	1.1398 0.002	<b>11090</b> 42 144.2 2
Ta-P7-7#4	56.1	<i>Acropora sp</i>	4.05	0.11056	0.00031	1.1411 0.002	<b>11061</b> 40 145.6 2
Ta-P7-7#5	56.1	<i>Acropora sp</i>	3.98	0.11055	0.00031	1.1409 0.002	<b>11062</b> 39 145.4 2
Ta-P7-8	59.2	<i>P. cf verrucosa</i>	2.50	0.11327	0.00033	1.1412 0.002	<b>11346</b> 41 145.8 2
Ta-P7-9	65.2	<i>P. cf verrucosa</i>	2.77	0.11518	0.00033	1.1399 0.002	<b>11563</b> 42 144.5 2
Ta-P7-10	65.5	<i>Porites sp.</i>	3.13	0.11929	0.00049	1.1395 0.002	<b>12004</b> 58 144.3 2
Ta-P7-11	72.1	<i>P. cf verrucosa</i>	2.32	0.12832	0.00039	1.1412 0.002	<b>12950</b> 49 146.4 2
Ta-P7-12	72.1	<i>Pocillopora sp</i>	2.61	0.12763	0.00036	1.1412 0.002	<b>12875</b> 46 146.4 2
Ta-P7-13	73.6	<i>Porites sp.</i>	2.67	0.12628	0.00067	1.1377 0.003	<b>12773</b> 81 142.7 3
Ta-P7-14	74.3	<i>Porites sp.</i>	2.75	0.12661	0.00052	1.1397 0.002	<b>12785</b> 62 144.8 2
Ta-P7-15	74.8	<i>Porites sp.</i>	2.77	0.12784	0.00051	1.1374 0.002	<b>12945</b> 61 142.5 2
Ta-P7-16	76.3	<i>Porites sp.</i>	2.66	0.12849	0.00053	1.1401 0.002	<b>12981</b> 63 145.3 2
Ta-P7-17	77.4	<i>Porites sp.</i>	2.68	0.13001	0.00036	1.1400 0.002	<b>13146</b> 47 145.3 2
Ta-P7-18#1	80.5	<i>Porites sp.</i>	2.76	0.13411	0.00068	1.1394 0.003	<b>13596</b> 85 144.8 3
Ta-P7-18#2	80.5	<i>Porites sp.</i>	2.74	0.13333	0.00053	1.1395 0.002	<b>13510</b> 64 144.9 2
Ta-P7-19#1	83.5	<i>A. gpe robusta/danai</i>	3.33	0.13633	0.00054	1.1379 0.002	<b>13856</b> 66 143.4 2
Ta-P7-19#2	83.5	<i>A. gpe robusta/danai</i>	3.33	0.13623	0.00055	1.1380 0.002	<b>13844</b> 68 143.5 3
Ta-P7-19#3	83.5	<i>A. gpe robusta/danai</i>	3.48	0.13558	0.00068	1.1383 0.003	<b>13769</b> 84 143.8 3
Ta-P8-162	37.9	<i>Acropora sp</i>	3.28	0.09668	0.00275	1.1418 0.002	<b>9594</b> 286 145.7 2
Ta-P8-176	40.2	<i>Pocillopora sp</i>	3.03	0.09721	0.00047	1.1427 0.001	<b>9642</b> 51 146.7 2
Ta-P8-182	41.5	<i>Pocillopora sp</i>	3.25	0.09788	0.00038	1.1425 0.002	<b>9713</b> 42 146.5 2
Ta-P8-203	44.2	<i>Favidea</i>	2.23	0.10228	0.00027	1.1418 0.001	<b>10179</b> 31 146.0 2
Ta-P8-222	46.7	<i>Acropora sp</i>	3.59	0.10316	0.00037	1.1427 0.001	<b>10262</b> 41 146.9 1
Ta-P8-232	49.0	<i>Acropora sp</i>	3.77	0.10543	0.00026	1.1413 0.001	<b>10514</b> 30 145.6 1
Ta-P8-244	51.4	<i>Pocillopora sp</i>	2.78	0.10704	0.00115	1.1426 0.002	<b>10670</b> 122 147.0 2
Ta-P8-260	52.9	<i>Acropora sp</i>	3.58	0.10752	0.00038	1.1416 0.002	<b>10730</b> 43 146.0 2
Ta-P8-269	54.9	<i>Acropora sp</i>	3.63	0.11142	0.00138	1.1418 0.001	<b>11140</b> 146 146.4 1
Ta-P8-269#2	55.0	<i>Acropora sp</i>	3.63	0.11038	0.00037	1.1417 0.001	<b>11031</b> 42 146.2 2
Ta-P8-295	63.3	<i>Pocillopora sp</i>	2.66	0.11852	0.00038	1.1408 0.001	<b>11902</b> 43 145.6 2
Ta-P8-299	68.3	<i>Pocillopora sp</i>	2.75	0.11988	0.00039	1.1451 0.002	<b>12004</b> 45 150.1 2
Ta-P8-307	70.7	<i>Favidea</i>	2.56	0.12128	0.00104	1.1453 0.001	<b>12149</b> 112 150.4 2
Ta-P8-319	73.1	<i>Porites sp</i>	2.64	0.12505	0.00046	1.1431 0.003	<b>12571</b> 59 148.3 3
Ta-P8-320	73.2	<i>Porites sp (branching)</i>	2.70	0.12536	0.00077	1.1438 0.003	<b>12596</b> 91 149.0 3
Ta-P8-322	73.3	<i>Porites sp (branching)</i>	2.58	0.12450	0.00062	1.1433 0.002	<b>12510</b> 70 148.5 2
Ta-P8-338	74.7	<i>Porites sp (branching)</i>	2.57	0.12681	0.00038	1.1414 0.001	<b>12780</b> 44 146.6 1
Ta-P8-348	74.7	<i>Pocillopora sp</i>	2.67	0.12835	0.00050	1.1409 0.002	<b>12956</b> 57 146.2 2
Ta-P8-353	83.0	<i>Porites sp</i>	3.17	0.13245	0.00039	1.1408 0.002	<b>13398</b> 47 146.2 2
Ta-P8-354	83.2	<i>Porites sp</i>	3.00	0.13204	0.00138	1.1402 0.002	<b>13356</b> 150 145.6 2
Ta-P8-359	85.4	<i>Porites sp</i>	2.19	0.13579	0.00040	1.1382 0.002	<b>13788</b> 49 143.7 2
Ta-P8-360	85.5	<i>Porites sp</i>	3.28	0.13639	0.00240	1.1394 0.002	<b>13837</b> 261 145.0 2
Ta-P8-362	85.6	<i>Porites sp</i>	3.37	0.13591	0.00039	1.1430 0.002	<b>13743</b> 47 148.7 2
Ta-P8-363	85.3	<i>Porites sp</i>	2.82	0.13558	0.00060	1.1393 0.002	<b>13756</b> 69 144.8 2
Ta-P8-365	86.8	<i>Porites sp</i>	2.42	0.13622	0.00060	1.1437 0.002	<b>13767</b> 68 149.4 2
Ta-P8-369	88.0	<i>Porites sp</i>	3.14	0.13568	0.00028	1.1363 0.001	<b>13801</b> 36 141.7 1
Ta-P8-372	87.6	<i>Acropora sp</i>	3.06	0.13708	0.00053	1.1385 0.002	<b>13929</b> 64 144.1 2
Ta-P9-200	53.2	<i>Acropora sp</i>	3.04	0.10991	0.00218	1.1427 0.001	<b>10971</b> 230 147.2 2
Ta-P9-200#2	53.3	<i>Acropora sp</i>	3.11	0.10807	0.00027	1.1414 0.001	<b>10790</b> 32 145.8 2
Ta-P9-213	58.2	<i>Acropora sp</i>	3.67	0.11391	0.00048	1.1438 0.002	<b>11386</b> 54 148.5 2
Ta-P9-231	64.6	<i>Porites sp</i>	2.79	0.12280	0.00039	1.1424 0.002	<b>12340</b> 46 147.5 2
Ta-P9-232	64.6	<i>Porites sp</i>	2.88	0.12217	0.00048	1.1418 0.001	<b>12279</b> 54 146.8 2
Ta-P9-233	65.7	<i>Porites sp</i>	3.14	0.12250	0.00050	1.1407 0.002	<b>12328</b> 57 145.7 2
Ta-P9-242	67.3	<i>Porites sp</i>	3.01	0.12483	0.00038	1.1421 0.001	<b>12559</b> 44 147.2 2
Ta-P9-242#2	67.3	<i>Porites sp</i>	2.93	0.12422	0.00082	1.1428 0.001	<b>12486</b> 89 147.9 2
Ta-P9-255	69.6	<i>Pocillopora sp</i>	2.60	0.12723	0.00071	1.1442 0.002	<b>12796</b> 78 149.5 2
Ta-P9-264	71.1	<i>Porites sp</i>	3.07	0.12862	0.00028	1.1443 0.001	<b>12943</b> 36 149.7 2
Ta-P9-265	73.3	<i>Porites sp</i>	3.06	0.12859	0.00039	1.1420 0.002	<b>12968</b> 47 147.3 2
Ta-P10-272	38.0	<i>Acropora sp</i>	3.12	0.10038	0.00207	1.1449 0.002	<b>9951</b> 216 149.0 2
Ta-P10-302	50.7	<i>Acropora sp</i>	3.69	0.10851	0.00081	1.1424 0.002	<b>10826</b> 87 146.8 2
Ta-P10-317	56.8	<i>Porites</i>	2.84	0.11300	0.00048	1.1404 0.001	<b>11321</b> 53 145.0 1
Ta-P10-321	57.0	<i>Acropora sp</i>	3.32	0.11363	0.00070	1.1399 0.002	<b>11393</b> 76 144.5 2
Ta-P10-332	61.9	<i>Favidea</i>	2.87	0.11717	0.00039	1.1410 0.002	<b>11756</b> 46 145.8 2
Ta-P10-333	61.9	<i>Porites</i>	2.92	0.11931	0.00074	1.1429 0.004	<b>11962</b> 93 147.8 5
Ta-P10-338	63.1	<i>Pocillopora sp</i>	2.50	0.11998	0.00049	1.1417 0.002	<b>12048</b> 55 146.6 2
Ta-P10-341	63.3	<i>Acropora sp</i>	3.48	0.12008	0.00060	1.1415 0.002	<b>12060</b> 67 146.4 2
Ta-P10-355	68.4	<i>Porites sp</i>	2.91	0.12290	0.00038	1.1401 0.002	<b>12377</b> 45 145.1 2
Ta-P10-372	74.7	<i>Porites sp</i>	2.67	0.12893	0.00050	1.1420 0.002	<b>13000</b> 57 147.3 2
Ta-P10-375	77.2	<i>Porites sp</i>	2.91	0.12971	0.00029	1.1418 0.002	<b>13086</b> 247 147.2 2
Ta-P10-373	77.2	<i>Porites sp</i>	2.80	0.13020	0.00039	1.1441 0.002	<b>13110</b> 47 149.6 2

Table S2	9-14 kyr BP	9-11.65 kyr BP	YD (11.65-12.85 kyr BP)	12.85-14 kyr BP
Tahiti (excl. <i>Porites</i> & <i>Favidea</i> , excl. lower part of P8)	10.3 ±0.2 R <sup>2</sup> =0.98	11.7 ±0.4 R <sup>2</sup> =0.96	7.5 ±1.1 R <sup>2</sup> =0.96	12.1 ±0.6 R <sup>2</sup> =0.99
Tahiti (all corals excl. lower part of P8)	10.2 ±0.2 R <sup>2</sup> =0.98	11.7 ±0.4 R <sup>2</sup> =0.96	9.9 ±1.4 R <sup>2</sup> =0.80	10.9 ±1.0 R <sup>2</sup> =0.90
Tahiti (excl. <i>Porites</i> & <i>Favidea</i> , incl. lower part of P8)	10.4 ±0.2 R <sup>2</sup> =0.98	11.7 ±0.4 R <sup>2</sup> =0.96	6.0 ±3.6 R <sup>2</sup> =0.48	12.4 ±1.1 R <sup>2</sup> =0.96
Barbados ( <i>A. palmata</i> only)	10.5 ±0.5 R <sup>2</sup> =0.96	8.4 ±0.6 R <sup>2</sup> =0.96	5.6 ±0.4 R <sup>2</sup> =0.97	9.3 ±0.4 R <sup>2</sup> =0.99
Barbados (YD excl. 11.5 kyr samples, see SOM-2)			5.5 ±0.9 R <sup>2</sup> =0.93	
Huon, Papua New-Guinea	9.4 ±0.8 R <sup>2</sup> =0.92	15.6 ±1.7 R <sup>2</sup> =0.95	10.4 ±1.7 R <sup>2</sup> =0.91	10.9 (2 pts)